Structure and Function of the Calcium Pump

David L. Stokes* and N. Michael Green**

* Skirball Institute of Biomolecular Medicine, Department of Cell Biology, New York University School of Medicine, 540 First Ave, New York, NY 10012, USA, stokes@saturn.med.nyu.edu

** National Institute of Medical Research, The Ridgeway, Mill Hill, London NW7 1AA, UK, mgreen@nimr.mrc.ac.uk

Keywords: Ion transport, Ca^{2+}-ATPase, reaction cycle, x-ray crystallography, electron microscopy

Short title: Structure and Function of Ca-ATPase

Corresponding author: David Stokes, Skirball Institute, NYU School of Medicine, 540 First Ave, New York, NY 10012, USA, tel. & fax: 212-263-1580, email: stokes@saturn.med.nyu.edu

ABSTRACT

Active transport of cations is achieved by a large family of ATP-dependent ion pumps, known as P-type ATPases. Various members of this family have been targets of structural and functional investigations for over four decades. Recently, atomic structures have been determined for Ca^{2+}-ATPase by x-ray crystallography, which not only reveal the architecture of these molecules, but offer the opportunity to understand the structural mechanisms by which the energy of ATP is coupled to calcium transport across the membrane. This energy coupling is accomplished by large-scale conformational changes. The transmembrane domain undergoes plastic deformations under the influence of calcium binding at the transport site. Cytoplasmic domains undergo dramatic rigid-body movements, that deliver substrates to the catalytic site and that establish new domain interfaces. By comparing various structures and correlating functional data, we can now begin to associate the chemical changes constituting the reaction cycle with structural changes in these domains.

HISTORICAL PERSPECTIVE

The control of ion balance across the cell membrane was originally the province of physiology, until almost fifty years ago when evidence began to emerge that ion gradients were created by ATP-driven cation pumps, opening the way to biochemical analysis. The pumps, or ATPases, were located mainly in the plasma membrane or in the internal membranes of the endoplasmic reticulum and the resulting gradients were used in a variety of signalling systems, mediated by gated ion channels. Although originally discovered in crab sciatic nerve (85), much of the early work on the sodium pump (Na^+/K^+-ATPase) used the resealed ghost of the erythrocyte as a model system (75). This was not a rich source of protein, but it allowed independent control over the ionic environments on either side of the membrane, thus providing a variety of ion exchange parameters (32). From the beginning, work on the calcium pump (Ca^{2+}-ATPase; 26) utilised the sarcoplasmic reticulum of muscle, a highly enriched source that is well suited to biochemical and structural studies. Parallel studies on Na^+/K^+-ATPase with the renal cortex, indicated that the two pumps employed largely similar reaction cycles; this, together with 35% identity in their amino acid sequences, provided the basis for founding the now rather large family of P-type ATPases (28). Extensive studies of kinetics and of the effects of chemical modification and site mutation have lead to an ever increasing understanding of pump function (reviewed by 61, 64). Nevertheless, fundamental questions related to energy transduction - in this case, the interconversion of chemical and osmotic energy - have only been approachable in the last two years, following the determination of two Ca^{2+}-ATPase structures by X-ray crystallography (93, 94). Together with cryoelectron microscopy, which provides lower resolution maps that can be modeled at an atomic level with the x-ray structures (51, 104), several conformations have so far been defined. This represents a good start in describing kinetic and chemical properties of the various reaction cycle intermediates in structural terms and thus in better understanding the molecular mechanism.

REACTION CYCLE

From a biochemical perspective, the reaction cycle for these pumps is characterized by alternating steps of ion binding and phosphate transfer (illustrated in Table I and reviewed in 21,

36, 62). The central event and the hallmark of this family of P-type ATPases is the formation of an acid-stable aspartyl phosphate intermediate. ATP is the preferred substrate for phosphoryl transfer, which is initiated by cooperative binding of two cytoplasmic calcium ions to transport sites. The energy of this phosphoenzyme is postulated to fuel a conformational change, which closes the ion gate from the cytoplasm, reduces the affinity of these transport sites for calcium and opens the ion gate toward the lumenal side of the membrane. After releasing calcium, protons are bound to the transport sites and the aspartyl phosphate is hydrolyzed to complete the cycle. A net exchange of protons for calcium results from the release of these same protons to the cytoplasm prior to binding the next pair of cytoplasmic calcium ions. The coordinated affinity change at the transport sites is the key to active transport as the cytoplasmic calcium ions are bound with μM affinity and released to the lumen with mM affinity.

In broad terms, energy transduction is accomplished by sequential changes in chemical specificity for phosphoryl transfer and in vectorial specificity for ion binding (44, 47). In particular, vectorial specificity refers to whether the pump binds ions from the cytoplasmic or from the lumenal side of the membrane and chemical specificity refers to whether the catalytic site reacts with ATP or with inorganic phosphate. Early kinetic models for Ca^{2+}-ATPase and Na^+/K^+-ATPase, postulated two distinct conformations dubbed E_1 and E_2 (1, 56, 76). The former was accessible to cytoplasmic ions and transferred phosphate to and from ATP, whereas the latter was accessible to extracellular/lumenal ions and reacted directly with inorganic phosphate. More recent models describe the cycle as a series of unique conformations transformed by sequential binding and release of substrates (46). A long-standing goal of structural studies has been to define these conformations and their interaction with the relevant substrates.

ELECTRON MICROSCOPY OF CA^{2+}-ATPASE AND OTHER P-TYPE ATPASES

Structural studies of both Ca^{2+}-ATPase and Na^+/K^+-ATPase were initiated in the early 1980's when it was discovered that 2D arrays could be induced within native membranes. In particular, vesicular preparations of porcine kidney Na^+/K^+-ATPase (87) and, later, Ca^{2+}-ATPase from rabbit sarcoplasmic reticulum (23) and H^+/K^+-ATPase from gastric mucosa (77) formed 2D arrays when incubated in vanadate-containing solutions that stabilized an E_2 conformation. Orthovanadate was used because of its characteristic inhibition of many P-type ATPases, presumably as a transition state analogue of phosphate during hydrolysis of E_2-P (22, 73). However, it was later discovered that decavanadate was actually responsible for Ca^{2+}-ATPase crystallization (48, 60, 96) and that the same Na^+/K^+-ATPase crystal form could also be induced by phospholipase A2 in the absence of vanadate (63). A variety of other 2D crystals were studied, including those from scallop adductor muscle in both E_2 (11) and E_2-P (35) conformations and from Na^+/K^+-ATPase stabilized by ATP analogues (86). In addition, both Ca^{2+}-ATPase (25) and H^+-ATPase (17) were crystallized in the E_1 conformation. Conditions for the former required both detergent and lipid and resulted in stacked crystalline layers with Ca^{2+}-ATPase molecules protruding symmetrically from either side, thus representing a very thin 3D crystal (89). These conditions were optimized to produce larger crystals that were analyzed extensively by electron diffraction (83, 84) and that were ultimately used for the x-ray crystallographic structure of $E_1 \cdot Ca_2$ described below.

These various preparations have resulted in numerous 2D and 3D structures by electron microscopy (EM) of Ca^{2+}-ATPase (57, 68, 95), Na^+/K^+-ATPase (37, 59, 79), H^+/K^+-ATPase (103) and H^+-ATPase (7) preserved first in negative stain and later in the frozen, unstained state. Early structures showed that the molecule had a compact, pear-shaped cytoplasmic head that was connected to the membrane by a thinner stalk. Structures of Na^+/K^+-ATPase showed protein domains on both sides of the membrane, consistent with the extracellular contribution of the β subunit. An ongoing controversy over the number of transmembrane helices was finally resolved by structures for Ca^{2+}-ATPase (106) and H^+-ATPase (7) at 8 Å resolution, which revealed ten transmembrane helices as originally predicted from the Ca^{2+}-ATPase sequence (55). Comparison of these structures (88), as well as projection structures from the thin, 3D crystals of Ca^{2+}-ATPase (68, 91), revealed large domain movements thought to characterize the conformational change between E_2 and E_1. Currently, the higher resolution EM structures are proving useful for fitting atomic coordinates determined by x-ray crystallography (51, 79, 104), thus elucidating different conformational states at an atomic level.

MOLECULAR ARCHITECTURE OF CA^{2+}-ATPASE

A major breakthrough for the field came from the x-ray crystal structure of Ca^{2+}-ATPase in the $E_1 \cdot Ca_2$ conformation (93). The resulting atomic model revealed four basic domains (Figs. 1 and 2). The transmembrane domain is almost entirely helical and includes the short loops on the lumenal and cytoplasmic surfaces; four of the transmembrane helices extend into the cytoplasm to form the stalk seen in earlier EM structures. The three cytoplasmic domains are derived predominantly from two large cytoplasmic loops between transmembrane helices M2/M3 and M4/M5. The latter loop forms the phosphorylation (P) domain, which sits directly on top of M4 and M5, and the nucleotide-binding (N) domain, which is itself an insert within the phosphorylation domain. These two domains are named for the ligands they carry, namely D^{351} that forms the phosphoenzyme and the site near K^{492} that binds ATP. The third cytoplasmic loop, dubbed the transduction or actuator (A) domain, comprises the smaller M2/M3 loop as well as the N-terminus.

Transmembrane Domain

The most important landmark of the transmembrane domain is the calcium binding site, which in the E_1 conformation cooperatively binds two calcium ions from the cytoplasm (Fig. 3a). The associated residues correspond remarkably well with those previously identified by site-directed mutagenesis. Initially, these residues were identified by phosphorylation of mutant pumps (15), which require calcium binding when performed in the forward direction with ATP, but not when performed in reverse using P_i. Later, the sequential nature of calcium binding was used to distinguish the two sites, because binding by the first calcium ion was sufficient to prevent phosphorylation from P_i, whereas binding by both calcium ions was required for phosphorylation from ATP. Thus, individual calcium site mutants displaying P_i phosphorylation that was insensitive to calcium were assigned to the first site, whereas those with normal sensitivity were assigned to the second site (3). This analysis was later corroborated by direct measurement of calcium binding stoichiometries in a more efficient expression system (92).

Specifically, the x-ray structure showed oxygen ligands for calcium provided by residues on M4, M5, M6, and M8. The first calcium ion was bound by N^{768} and E^{771} on M5, T^{799}, D^{800} on M6 and E^{908} on M8. The contribution of adjacent residues along M6 was aided by flexibility in this helix due to the non-helical hydrogen bonding of carbonyl oxygens of N^{799} and D^{800}. The second ion binding site was quite different, with extensive contributions from main-chain carbonyl oxygens along M4 as well as side-chain oxygens from E^{309} on M4 and N^{796} and D^{800} on M6. A highly conserved sequence motif on M4 ($PEGL^{311}$) lies at the heart of this second site and likely represents the key to cooperativity. In particular, binding of the first ion to M5/M6/M8 must somehow induce the favorable configuration of M4 to provide for the cooperative binding of the second ion. This implied structural flexibility of M4, as well as its direct link to the phosphorylation site, place these particular structural elements at the center of the global conformational change that accompanies calcium binding to the enzyme.

Phosphorylation Domain

Phosphorylation occurs on an aspartate ~30 residues beyond the C-terminal end of M4 in a highly conserved region that serves as a signature sequence for P-type ATPases: $DKTGT^{355}$. Initially, this phosphorylation site was identified by chemical means; later, site-directed mutagenesis of the aspartate and its conserved neighbors was shown to interfere specifically with phosphorylation (2). The specific fold of the P domain had previously been deduced by analogy with bacterial dehalogenases and used to define a superfamily of hydrolases which also included small molecule phosphatases (5). This deduction relied on an alignment of several short, highly conserved sequences that were known to play key roles in the catalytic sites of all these enzymes: $DKTGT^{355}$, KSK^{686}, TGD^{627}, and $DGVND^{707}$ (Fig. 1). The resulting structural prediction consisted of a Rossmann fold with an inserted ATP-binding domain and was found to be consistent with predictions of secondary structure and with effects of mutagenesis and chemical modification throughout both domains (90). A common catalytic mechanism was also implied by the fact that the nucleophilic aspartate (D^{351}) of both dehalogenases and phosphatases form a covalent intermediate during the reaction cycle (16). These predictions were confirmed by the x-ray structure of Ca^{2+}-ATPase, which revealed not only a Rossmann fold, but also a common arrangement of catalytic site residues (Fig. 4) relative to both dehalogenases (39) and phosphatases (100).

Although the Rossmann fold represents the template for this phosphorylation domain, Ca^{2+}-ATPase has several adaptations relevant to the energy coupling required for calcium transport. The fold is characterized by a central, six-stranded parallel β-sheet flanked by three α-helices on each side (Figs. 1 & 4). As predicted from the sequence of Ca^{2+}-ATPase, the α-helices alternate with the β-strands along the peptide chain. Typical of α/β structures, the active site exists at the topological break point dividing the first three strands from the last three strands and critical residues appear in the loops between each strand and the subsequent helix (10). The most important loop, that following the phosphorylated aspartate, is interrupted by the nucleotide-binding domain. The discontinuous pieces of this loop have the most highly conserved sequences of the family, namely the signature sequence $DKTGT^{355}$ following the phosphorylation site and $DPPR^{604}$ in the return from the nucleotide-binding domain. The P domain is firmly connected to the transmembrane domain by cytoplasmic extensions of M4 and M5 (S4 and S5). In the case of S5, its cytoplasmic extension represents one of the six flanking

helices of the Rossmann fold. S4 represents an extra structural element, which is followed by a short, antiparallel β-strand and α-helix leading to the beginning of the Rossmann fold. This preliminary β-strand extends the central β-sheet and probably serves to couple movements of M4 to those of the phosphorylation domain, as described below. The preliminary α-helix, dubbed P1, runs underneath the Rossmann fold and interacts with lower parts of S5 as well as with the loop between M6 and M7, thus also potentially coupling movements of the membrane components with those of the phosphorylation domain. Finally, there is an insert consisting of a strand and two short helices (P4a and P4b) on the other end of the Rossmann fold. This insert is on the periphery of the structure and is highly variable amongst P-type ATPases, being considerably larger in Na^+/K^+-ATPase and absent in CadA (90).

Nucleotide-binding domain

The N domain represents a novel fold comprising a 7-stranded, antiparallel β-sheet sandwiched between two helix bundles (Fig. 2a). The nucleotide site is tucked under a flap created by one of the α-helices. This site was identified by soaking TNP-AMP into the crystals (93) and is generally consistent with site-directed mutagenesis and chemical modification of nearby residues F^{487}, K^{492} and K^{515} (2, 8). However, the binding geometry of ATP may be different given that the TNP moiety produces a large increase in affinity and, in the case of TNP-ATP, prevents transfer of γ-phosphate to the catalytic aspartate (101). In any case, the most striking observation is the large distance between this site and the target aspartate (>25Å), which makes phosphate transfer impossible in this conformation. Given the apparent flexibility of the loops connecting P and N domains, significant mobility of the N domain has been suggested (104), which is consistent with systematic changes in glutaraldehyde crosslinking of these domains (Table I) and with direct measurements of the rotational dynamics of the N domain (41). Furthermore, various fluorescence probes and cysteine reactivity indicate lowered solvent exposure of the nucleotide-binding site upon phosphorylation (Table I, 8, 66). A variety of indirect structural evidence also supports the mobility of the N domain. In particular, the 3D crystal packing of Ca^{2+}-ATPase in the $E_1 \cdot Ca_2$ conformation is variable (14) and comparisons of the x-ray structure with a cryoEM projection map from this same crystal form (68) suggests that this variability is due to different angles between N and P domains. Also, both the N and A domains have variable orientations in a variety of 3D structures of Ca^{2+}-ATPase, Na^+/K^+-ATPase and H^+-ATPase (e.g., Fig. 2).

Actuator or transduction domain

The third cytoplasmic domain, which was originally called the transduction domain and later the nose, β-strand and actuator domain, is composed primarily of β-strands, which form a distorted jelly roll and which are tethered to M2 and M3 by two flexible, unstructured loops (Figs.1 and 2). Two α-helices are packed against this jelly roll, which come from the N-terminus of the pump and which are connected by another long, unstructured loop to M1. The characteristic $TGES^{184}$ motif is on an exposed loop in the original x-ray crystal structure, but large reorientation of this domain in other conformations give this motif a plausible role in catalysis, as implied by mutagenesis studies of these residues (2). Experimental evidence for this reorientation comes primarily from the conformational dependence of proteolytic cleavage. In particular, the tryptic site at R^{198} near the $TGES^{184}$ loop (42, 49) as well as a variety of cleavage

sites in the flexible loop of Ca^{2+}-ATPase and Na^+/K^+-ATPase leading to M3 (50, 65) undergo rapid proteolysis in the $E_1 \cdot Ca_2$ conformation relative to the E_2 conformation.

STRUCTURAL CHANGES INDUCED BY CALCIUM BINDING

As stated, a major goal of structural studies has been to elucidate changes which accompany the reaction cycle of the pump. The most recent x-ray structure takes a big step in this direction by revealing the E_2 conformation of Ca^{2+}-ATPase stabilized by thapsigargin in the calcium-free state, dubbed the $E_2 \cdot TG$ conformation (94). As expected by earlier comparisons with E_2 structures by cryoEM (91, 93, 104), this conformation has very large changes relative to $E_1 \cdot Ca_2$. In particular, the three cytoplasmic domains undergo large, rigid-body movements, namely a 110º rotation of the A domain about an axis normal to the membrane, a 30º rotation of the P domain with respect to the membrane plane, and a further 50º rotation of the N domain relative to the P domain. These large scale movements were anticipated in a general way by a host of earlier spectroscopic, enzymatic and biochemical studies (45) and result in a compact cytoplasmic head that contrasts with the markedly open structure of $E_1 \cdot Ca_2$ (Fig. 2). Even with their closer association, the interactions between the cytoplasmic domains in $E_2 \cdot TG$ are rather weak and therefore potentially labile during the reaction cycle. Interestingly, the structure within individual cytoplasmic domains is largely unchanged. Although this observation is consistent with the very small changes in secondary structure measured by circular dichroism (31), one might have expected some differences at the phosphorylation site to account for its activation after calcium binding.

In contrast to the rigid body movements of the cytoplasmic domains, the transmembrane domain undergoes extensive deformations along most of its helices. As might be expected, the configuration of side chains surrounding the calcium sites is significantly different in the absence of these ions (Fig. 3b). In particular, loss of calcium ligands causes M6 to unwind, resulting in a 90º rotation of relevant side chains: N^{796}, T^{799}, and D^{800}. M4 shifts down almost 5 Å and the side chain of E^{309} rotates completely away from the site to face M1. A dramatic bend in M1 pulls E^{58} out of the site altogether (Fig. 2c). E^{771} and E^{908} in M5 and M8 do not change much, though N^{768} rotates ~30º toward M4. To be sure, the resulting withdrawal of calcium ligands from this site appears to justify the 1000-fold decrease in calcium affinity in the E_2 conformation. Toyoshima and Nomura go further and postulate that this particular arrangement of sidechains reflects the evolutionary relationship with Na^+/K^+-ATPase, which would require liganding of two potassium ions at this stage of its reaction cycle (94).

These localized changes at the calcium sites give rise to a larger set of deformations in helices M1-M6, many of which were deduced in fitting the original x-ray structure to a cryoEM map of the $E_2 \cdot VO_4$ conformation (104). Most of these deformations involve bending or tilting of helices, which depending on the axis of tilt imparts a rocking motion causing several helices to move up or down relative to the bilayer. Perhaps the central movement is the bending of the cytoplasmic end of M5 about a pivot point centered at G^{770}. Because the top of M5 is integrated into the Rossmann fold at the heart of the P domain, the bending of M5 could plausibly induce rotation of the P domain as a whole. Given its rigid link to M4, P domain rotation causes a rocking of M4 about the same pivot point as M5 (G^{770}), producing the observed displacement of M4 normal to the bilayer. M3 undergoes a combination of rocking and bending, such that M3 and M5 end up bowed towards one another in the absence of calcium; both are straight and parallel to one another in $E_1 \cdot Ca_2$. Given the minimal interaction between M3 and the P domain,

the changes in M3 are likely induced by van der Waals interactions with M4 and M5 within the bilayer and by interactions between the lumenal loops L34 and L78 (discussed below). Intriguingly, M1 and M2 are connected to the A domain only by flexible loops, yet undergo even larger movements. In the case of M2, there is an inclination about a pivot point at the lumenal end of this long helix, as well as partial unwinding at the cytoplasmic end in E_2·TG. M1 is displaced >10 Å laterally, shifted upwards, and bent 90º at the cytoplasmic surface of the bilayer thus pulling E^{58} away from the calcium sites in E_2·TG. Finally, the L67 loop can be considered part of the transmembrane domain and is H-bonded both to the cytoplasmic part of M5 (S5) and to one of the helices in the P domain; thus, a modest movement of this loop is coupled to the rotation of the P domain and the bending of M5. The fact that M7-M10 remain relatively unchanged is consistent with their absence in the subfamily of P-type ATPases specializing in so-called soft-metal ions like copper, zinc and cadmium (54).

STRUCTURAL EFFECTS OF PHOSPHORYLATION

Although there are no x-ray structures for the phosphorylated forms of Ca^{2+}-ATPase, electron microscopy has been used to solve a series of structures at intermediate resolution, the latest of which was used to build an atomic model (104). The conformation represented by this structure has been controversial. Initially, the vanadate used for inducing the tubular crystals used for these studies was assumed to stabilize E_2-P (24), but it was later discovered that decavanadate, not orthovanadate, was actually the effector for crystallization (60, 96). Also, vanadate-free conditions were sufficient for crystallization of the scallop isoform of Ca^{2+}-ATPase (11) and the ability of thapsigargin to promote crystallization was initially ascribed to its trapping of the E_2 conformation (81). Nevertheless, more recent studies of thapsigargin document its interaction with E_2-P (82) and proteolysis studies (19) now suggest that the EM structures are indeed representative of E_2-P or E_2·PO_4. Decavanadate appears to occupy two positions in the crystals, one extramolecular site mediating a crystal contact between two-fold related molecules and a second, intramolecular site in between the N and A domains (90). This second site was confirmed by crystallizing Ca^{2+}-ATPase labelled by FITC, which displaced the intramolecular decavanadate and left a corresponding hole in the density map between these domains (104). Although not visible at these resolutions, orthovanadate is undoubtedly also present in these solutions and presumably acts as a transition state analogue at the catalytic site. Finally, a truly phosphorylated form of Ca^{2+}-ATPase can be prepared from the FITC-labelled enzyme (13). After stabilizing this species with thapsigargin, tubular crystals can be readily formed by decavanadate (38) and the structure closely resembles that of the unmodified enzyme (D. Stokes, F. Delavoie, J.-J. Lacapere, unpublished results). Taken together, these data suggest that EM structures from the vanadate-induced tubular crystals are indeed representative of E_2-P, providing a nice complement to the x-ray structures of E_2·TG and E_1·Ca_2 conformations.

The atomic model for E_2·VO_4 was built by fitting atomic coordinates for E_1·Ca_2 to this the EM density map at 6 Å (104). The three cytoplasmic domains were fitted individually as rigid bodies, whereas the helices composing the membrane domain were bent and displaced to match the corresponding density in the map. The transmembrane and P domains of the resulting structure are rather similar to E_2·TG, despite some spurious displacements of individual transmembrane helices along their axes due to the limited resolution of the EM map. In contrast, the N domain is significantly more vertical, allowing the A domain to more closely approach the

P domain in the $E_2 \cdot VO_4$ structure (Fig. 5). This difference appears to reflect differing interactions between the conserved sequences $TGES^{184}$ and $DGVND^{707}$, which mediate the interface between A and P domains in $E_2 \cdot TG$. As described below, these differences may be due to orthovanadate at the active site, indicating that the position of the A domain is sensitive to formation and hydrolysis of the aspartyl phosphate. Given the documented flexibility of the N domain, it seems likely that its different position in $E_2 \cdot TG$ and $E_2 \cdot VO_4$ structures is governed primarily by the A domain, with which it has the most extensive contacts.

STRUCTURAL EFFECTS OF THAPSIGARGIN

There has been much interest in characterizing the effects of thapsigargin, a plant sesquiterpene that binds with exceedingly high affinity and specificity to the SERCA1 isoform of Ca^{2+}-ATPase. Initial enzymatic studies suggested that thapsigargin reacts with the calcium-free, E_2 state to form a dead-end complex, which is then inert with respect to both calcium and P_i (81). Subsequent studies concluded that thapsigargin can in fact react with other enzymatic intermediates, namely $E_1 \cdot Ca_2$ (102) and E_2-P (82). In the latter case, measurements of ^{18}O exchange indicated that thapsigargin affected the stability of the aspartyl phosphate. Furthermore, thapsigargin appears to bind to the stable phosphorylated intermediate produced by FITC labelled Ca^{2+}-ATPase, making the phosphoenzyme stable for periods up to a week (38). A series of mutagenesis studies implicated a region at the cytoplasmic border of the M3 helix between residues 254-262 (107). A contradictory result was obtained by EM of crystals in the presence and absence of thapsigargin, which found consistent density differences at the lumenal side of the membrane between M3/M4 and M7/M8 loops, which were assigned to thapsigargin (105). The x-ray structure for $E_2 \cdot TG$ supported the mutagenesis data by showing thapsigargin bound near the cytoplasmic border in a crevice between M3, M5 and M7. Although still speculative, inhibitory effects of thapsigargin are likely to involve a general rigidification of these transmembrane helices, thus preventing them from conveying the conformational changes associated with calcium binding. In addition, this x-ray structure showed that the M3/M4 and M7/M8 loops moved substantially closer together relative to the $E_1 \cdot Ca_2$ structure in a way that could explain the difference density observed by EM. Toyoshima and Nomura suggested that these loops controlled the access of transport sites to the lumenal side of the membrane (94). However, the EM result suggests that thapsigargin influences these loops in the $E_2 \cdot VO_4$ crystals and it would therefore be important to determine their disposition in the uninhibited enzyme and to further study their role in calcium gating.

ACCESS TO THE CALCIUM SITES

Although the structures define the architecture of the calcium sites, they do not show clear entrance and exit paths. In the classic E_1/E_2 model, the sites of E_1 would be oriented toward the cytoplasmic side of the membrane, whereas in E_2 they would face the lumen. More recent analyses, based primarily on the lack of competition between lumenal and cytoplasmic calcium in formation of $E_1 \sim P$, suggest that calcium sites face the cytoplasm in both E_1 and E_2 and that it is phosphoenzyme formation which serves to reorient these sites (46). The x-ray structure of $E_2 \cdot TG$ supports this latter model by revealing potential access for ions from the cytoplasm, but not from the lumen. In particular, a negatively charged tunnel is visible between M1, M2 and M3, though it is blocked at the bottom by E^{309}. Given the relatively low pH (6) of

crystallization, this structure likely represents $E_2 \cdot H_3$ (Table I) and it is possible that deprotonation of E^{309}, which must precede calcium binding, initiates structural rearrangements to deliver calcium to the site. Although the cryoEM-based model for *Neurospora* H^+-ATPase in the E_1 conformation also reveals a plausible ion path via conserved polar side chains along M1 and M2 (51), mutagenesis of several glutamate residues along M1 failed to produce any effects on calcium binding by Ca^{2+}-ATPase (27). Also, movements of M1 and M3 block this tunnel in the $E_1 \cdot Ca_2$ structure, creating an inconsistency with the documented exchangeability of calcium by this intermediate. A potential pathway for release of calcium to the lumen was seen at much lower resolution in EM maps of the $E_2 \cdot VO_4$ structure (106). This pathway starts near the calcium sites and becomes quite wide as it approaches the M3/M4 and M7/M8 loops postulated to act as ion gates toward the lumen. This pathway potentially corresponds to a water-filled tunnel that has been proposed to explain voltage effects on sodium binding to Na^+/K^+-ATPase from the extracellular side of the membrane (30).

BIOCHEMICAL STUDIES OF CONFORMATIONAL CHANGE

Over the past 25 years, a wide variety of biochemical and biophysical techniques have been used to follow conformational changes (Table I) and it is now important to evaluate their results in light of the existing high resolution structures. On the one hand, these results will help validate the use of artificially stabilized intermediates for crystallographic studies and also fill in information about transient intermediates. On the other hand, comparison will enhance our understanding of these methods and thus facilitate their use in future work.

Changes in the reactivity of sulfydryl groups were studied in several early investigations using the reagent DTNB to define sub-classes of the 24 cysteine residues. Although it was not possible to assign rate constants to specific residues, three grades of reactivity have been assigned in Table I, allowing a number of general conclusions. About eight of the cysteines were unreactive in the absence of detergents, most likely corresponding to the six residues in transmembrane helices plus the disulfide linked pair in L78 (18). The remaining sulfydryls were scattered throughout the N and P domains, with only a single cysteine in the A domain, near the N-terminus. None were associated with the conserved catalytic loops of the P domain. The changes in reactivity appeared to affect whole classes of cysteines rather than isolated residues, probably reflecting global movements of the N and P domains, and maximal reactivity was obtained with $E_1 \cdot Ca_2$, consistent with its open structure. Over half the reactive cysteines suffered a 70% fall in reactivity when ATP analogues were bound and had even lower reactivity following phosphorylation.

The formation of a crosslink by glutaraldehyde between R^{678} in the P domain and K^{492} near the adenosine binding region of the N domain is also conformation dependent and has given useful information about the proximity of these domains (80). After crosslinking, the affinity for ATP decreased 1000-fold, without affecting calcium binding, phosphorylation by acetyl phosphate, or calcium occlusion. The next step, $E_1 \sim P$ to E_2-P, was completely blocked, consistent with the idea that the A domain could not be reoriented after coupling the N and P domains. Crosslinking was most efficient in $E_1 \sim P$, reflecting the close approach of N and P domains during phosphate transfer, and slower in $E_1 \cdot Ca_2$, supporting the mobility of the N domain. The distance between crosslinked residues in the $E_2 \cdot TG$ structure is significantly less

than in the $E_2 \cdot VO_4$ structure, consistent with the ability to form a crosslink in E_2 and not E_2-P. Furthermore, crosslinking blocks phosphorylation of E_2 with P_i, indicating that the observed movements of N and A domains are a necessary adjustment to the presence of the phospho group in the catalytic site.

Oxidative cleavage by iron has been effectively used to investigate the proximity of loops within the catalytic site of Na^+/K^+-ATPase (71). In these experiments, the iron substitutes for magnesium at the phosphorylation site and under oxidizing conditions cleaves nearby peptide bonds. Sites of cleavage have been identified in the catalytically important loops of the P domain and, perhaps most importantly, in the TGES loop of the A domain. In particular, cleavage of the TGES loop only occurs in E_2-P and $E_2 \cdot K$, supporting the docking of the A domain next to the P domain in these conformations. Further evidence for this docking comes from numerous proteolytic cleavage studies, which show sensitivity of several sites within the A domain in $E_1 \cdot Ca_2$, but not in E_2 conformations (50, 65).

A variety of fluorescent labels have been used to study conformational changes. The best characterized labels are TNP nucleotides, which show a large increase in fluorescence after phosphorylation, and NBD and FITC, which have both been used to monitor the E_1/E_2 equilibrium. In addition, advances in IR difference spectroscopy now allow individual residues or even specific bonds to be studied in the course of the reaction cycle (7a). In future studies, these probes may be useful in monitoring pump dynamics and deducing the structure of intermediates that are not accessible to structural studies.

STRUCTURAL MECHANISM OF TRANSPORT

Given the abundant structural and biochemical evidence for conformational changes, we are now faced with describing how these changes couple the local effects of calcium on the transmembrane sites to phosphorylation of D^{351} some 40 Å away. For some time, the M4/S4 connection between E^{309} and D^{351} has been discussed as most likely to mediate cross-talk between these sites (45). The x-ray structures show us that the links between the P domain and both M4 and M5 are indeed well-structured and potentially capable of conveying long-range conformational changes. Nevertheless, the actual sequence of events between binding of calcium and domain movement is still a matter for educated guesswork, guided by the conformational criteria in Table I .

In the starting conformation, calcium ligands are protonated ($E_2 \cdot H_3$) and a distinct step of deprotonation is required prior to binding cytoplasmic calcium. This step must involve opening the partially occluded proton sites seen in the $E_2 \cdot TG$ structure to the cytoplasm, e.g., by reorientation of E^{309}, and has been followed by kinetic studies of NBD fluorescence (97). This probe labels the P1 helix wedged between the top of M4 and the P domain and the fluorescence changes indicate that there must be some structural change in this region. However, the T2 tryptic cleavage site in the A domain is still protected at pH 7, even in the presence of nucleotide, indicating that the A domain is still docked with the P domain in this deprotonated state (20, 43). Thus, a high pH, calcium free conformation, which has typically been called E_1, appears to be intermediate between $E_2 \cdot H_3$ and $E_1 \cdot Ca_2$ with cytoplasmically exposed calcium sites but with the

A domain still in the E_2 conformation. Its properties may prove important in defining an access pathway for calcium, which has been problematic from the two existing x-ray structures.

In contrast to NBD, increases in tryptophan fluorescence (12) and small changes in circular dichroism (31) respond only to the actual binding of calcium to E_1 and are probably correlated with the cooperative changes required to create the second calcium site, whose occupation activates phosphorylation. From a structural point of view, these changes must induce unbending of M5 and displacement of M4, which according to the x-ray structures seem to represent levers for rotating the P domain, but the mechanism is not obvious. Locally, M6 undergoes the largest structural rearrangement with the backbone winding up upon calcium binding (Fig. 3). Perhaps this winding puts strain on the L67 loop which then induces the bending of M5. Binding of calcium by M4 might also induce its vertical movement as the main-chain carbonyls in its unwound portion move upward towards D^{800} to provide ligands for cooperative binding of the second calcium ion.

In subsequent steps of the reaction cycle, the P domain is clearly the center of operations and is seen to adopt two distinct orientations in response to calcium binding. In the presence of calcium, the P domain appears to be available for phosphate transfer from ATP bound within the N domain. In the absence of calcium, the P domain is seen to interact with the $TGES^{184}$ loop of the A domain. Thus, it is possible that movement of the P domain represents a kind of switch, under control of calcium binding that selects between the N and the A domains. This simple pivot might represent the mechanism for calcium-induced activation of D^{351} for phosphorylation, which cannot otherwise be explained by rearrangement of residues within the catalytic site (Fig. 4a). Although we do not have a structure of a phosphorylated intermediate, we postulate that consequent changes in the P domain would facilitate its interaction with the A domain and that formation of this A-P domain interface would represent the E_1~P to E_2-P transition that lowers calcium affinity and induces calcium release to the lumen.

In contrast to the P domain, the N and A domains are covalently tethered by flexible, unstructured loops and their noncovalent interactions with other cytoplasmic domains appear to be transient. Although there is convincing evidence for mobility of N and A domains, there is little indication of what causes their dramatic movements. A likely answer is thermal energy, or Brownian motion, which has been hypothesized as a driving force in the mechanisms of a wide variety of other macromolecular motors like F_oF_1 (70), myosin (40), kinesin (6), as well as protein translocation into mitochondria (69) and the endoplasmic reticulum (58). Thermal energy would ensure that these weakly bound and flexibly tethered domains would be moving extensively, thus sampling a large range of orientations and potential binding interfaces. In the absence of tethers, these domains could be viewed as separate subunits as seen, for example, in the family of response regulators, though the increased efficiency of a covalently attached domain should be advantageous for the continual turnover of ion pumps.

The specific changes which accompany phosphorylation must be precipitated by local events near D^{351} and, by analogy with G-protein switching (34), may well involve changes in the liganding of magnesium. Initially the magnesium is bound by two oxygens from the β and γ phosphates of ATP and by four other ligands provided by the protein (including bound waters). Analogy with the x-ray structures of phosphoserine phosphatase (99) suggests that ligating

oxygens of Ca^{2+}-ATPase would come from the phosphate, the D^{351} carboxyl, the D^{703} carboxyl, the T^{353} main-chain carbonyl and two from bound water molecules (Fig. 4). Homologous ligands are also found for several members of the CheY response regulator family (53) and appear to be consistent in an unpublished structure for the Mg_2F_4 complex of the Ca^{2+}-ATPase (Toyoshima & Nomura) and with mutagenesis of the $DGVND^{707}$ loop of Na^+/K^+-ATPase (72). Initially, magnesium bound by Ca^{2+}-ATPase is freely exchangeable (78), but after transfer of phosphate to D^{351} and loss of ADP, the magnesium becomes tightly bound ($k_{off} < 0.5\ s^{-1}$) and is released only after hydrolysis (98); similar results have been obtained with Na^+/K^+-ATPase (29). This represents a substantial difference from the phosphatases and response regulators, which bind magnesium loosely throughout their reaction cycles. We have previously suggested (90) that this "occlusion" of magnesium by Ca^{2+}-ATPase could imply a change in its ligation, which could initiate further conformational changes required for calcium occlusion and the E_1~P to E_2-P transition. It now seems likely that formation of the A-P domain interface may stabilize the magnesium ligand cage and that these interactions might induce further conformational changes within the transmembrane domain.

In the CheY family, a modest conformational change of the α-4, β-4 loop (homologous to TGD^{627} of Ca^{2+}-ATPase) follows formation of a new H-bond to the covalently linked phosphate and induces interactions with responsive subunits (e.g. FliM and CheZ). A similar effect may be occuring in the $DGVND^{707}$ loop in Ca^{2+}-ATPase, which is significantly farther from D^{351} than the analogous loop from response regulators and phosphatases (Fig. 4). We hypothesize that the presence of $Mg{\cdot}PO_4$ will pull this loop closer to provide the requisite ligands, thus producing a binding site for the $TGES^{184}$ loop from the A domain, which would in turn confer tighter magnesium binding. In terms of the reaction cycle, phosphoenzyme formation and movement of the $DGVND^{707}$ loop would produce the ADP-sensitive E_1~P intermediate and the docking of the A domain would initiate the transition to E_2-P.

The elements of this A-P domain interface include the conserved $TGES^{184}$ and $DGVND^{707}$ loops as well as the P6 helix and the $MAATEQ^{244}$ loop connecting the A domain to M3. The P6 helix directly follows $DGVND^{707}$ and contains K^{712}, which makes H-bonds with M^{239}, T^{242} and Q^{244} in the $E_2{\cdot}TG$ structure. Significantly, this $MAATEQ^{244}$ region contains proteolytic cleavage sites that are only accessible in the E_1 conformations (42, 50), consistent with its burial at a domain interface in E_2. Both mutagenesis of $TGES^{184}$ (2) and excision of the $MAATE^{243}$ sequence with proteinase K (65) yield enzymes defective in the E_1~P to E_2-P transition. Results of Fe-catalyzed cleavage of Na^+/K^+-ATPase place $TGES^{184}$ near the magnesium sites in E_2-P (71). Taken together, these results indicate that rotation of the A domain and formation of the A-P domain interface is essential for producing E_2-P. It is tempting to speculate that $TGES^{184}$ contributes ligands to the aspartyl-$PO_4{\cdot}Mg$ complex, similar to Q^{147} of CheZ, which ligates magnesium at the active site of CheY and ultimately directs a water molecule to hydrolyze the aspartylphosphate (108). Although the original analyses of $TGES^{184}$ mutations showed no change in phosphorylation levels either from ATP or from P_i (4), more thorough studies of magnesium binding might now be possible using larger scale expression systems.

Both the formation of E_2-P and its subsequent hydrolysis are linked to events at the calcium transport sites. The corresponding 90-110º rotation of the A domain is likely to place

stress on M1, M2 and M3 thereby accounting for their large movements in $E_2 \cdot VO_4$ and $E_2 \cdot TG$ structures. These movements may represent an indirect mechanism for altering the calcium binding properties, by opening the lumenal gate in the M3/M4 loop and by perturbing the ion binding sites between M4, M5, M6 and M8. The dramatic changes in E^{58} probably reflect this perturbation as this residue is H-bonded to E^{309} in $E_1 \cdot Ca_2$, but is pulled completely out of the site in $E_2 \cdot TG$ due to the kinking of M1 (Figs. 2c, 3), perhaps destabilizing E^{309} as a first step in lowering calcium affinity. Release of the calcium ions and/or protonation of the transport sites stimulates hydrolysis of E_2-P and, in analogy with the postulated effects of calcium binding, this signal is likely to be propagated through the M4/M5 helices and the L67 loop, perhaps inducing changes in the A-P domain interface like those seen in the structure of $E_2 \cdot TG$ relative to $E_2 \cdot VO_4$.

CONCLUDING REMARKS

The early description of E1 and E2 conformations of Ca^{2+}-ATPase (56) was of great help in sorting out the complexities of the cycle, but it is now worth considering whether they represent an oversimplification. To start, the switching of calcium sites envisioned by this model now seems to be incorrect, given both kinetic and structural evidence indicating that access by lumenal calcium is blocked in E_2. From the structural evidence, it might be concluded E_1 and E_2 conformations are distinguished from the location of the A domain, either engaged or disengaged from its docking site with the P domain. However, spectroscopic studies of calcium binding suggest that cytoplasmic domain movements occur upon binding calcium by the E_1 species, not during the deprotonation of $E_2 \cdot H_3$ that produces E_1. Thus, it may be more accurate to describe the reaction cycle as a series of unique intermediates separated by small, reversible steps. This view is certainly consistent with the energetics of the cycle under physiological conditions, which shows most steps to be separated by <10 kJ/mole (52), making them difficult to stabilize for structural studies. The alternative has been to use non-physiological ligands to trap certain intermediates, but this practice runs the risk of generating conformations that differ from those of the physiological intermediates. Some of these ligands cause the cytoplasmic domains to appear to behave independently from the calcium binding site. For example, glutaraldehyde crosslinking of N and P domains has no effect on calcium binding and the phosphoenzyme stabilized by FITC has high-affinity, cytoplasmically accessible calcium sites, but is still able to bind thapsigargin and form vanadate-induced 2D crystals. This behavior may tell us something about the structural coupling of the molecule, but also threatens to deceive us about the structural events of the reaction cycle. With this risk in mind, we should now turn our attention to using the several existing structures of Ca^{2+}-ATPase as a guide for formulating more precise experiments to either validate their relevance or to test the true nature of the physiological intermediates.

LITERATURE CITED

1. Albers R. 1967. Biochemical aspects of active transport. *Ann. Rev. Biochem.* 36:727-56

2. Andersen JP. 1995. Dissection of the functional domains of the sarcoplasmic reticulum Ca^{2+}-ATPase by site-directed mutagenesis. *Bioscience Reports* 15:243-61

3. Andersen JP, Vilsen B. 1994. Amino acids Asn796 and Thr299 of the Ca-ATPase of sarcoplasmic reticulum bind Ca at different sites. *J. Biol. Chem.* 269:15931-36

4. Andersen JP, Vilsen B, Leberer E, MacLennan DH. 1989. Functional consequences of mutations in the beta-strand sector of the Ca^{2+}-ATPase of sarcoplasmic reticulum. *J. Biol. Chem.* 264:21018-23

5. Aravind L, Galperin MY, Koonin EV. 1998. The catalytic domain of the P-type ATPase has the haloacid dehalogenase fold. *Trends Biol. Sci.* 23:127-29

6. Astumian RD, Derenyi I. 1999. A chemically reversible Brownian motor: application to kinesin and Ncd. *Biophys. J.* 77:993-1002

7. Auer M, Scarborough GA, Kühlbrandt W. 1998. Three-dimensional map of the plasma membrane H^+-ATPase in the open conformation. *Nature* 392:840-43

7a. Barth A, Zscherp C. 2000. Substrate binding and enzyme function investigated by infrared spectroscopy. *FEBS Lett*. 477:151-55

8. Bigelow DJ, Inesi G. 1992. Contributions of chemical derivatization and spectroscopic studies to the characterization of the Ca^{2+} transport ATPase of sarcoplasmic reticulum. *Biochim. Biophys. Acta* 1113:323-38

9. Bishop JE, Nakamoto RK, Inesi G. 1986. Modulation of the binding characteristics of a fluorescent nucleotide derivative to the sarcoplasmic reticulum adenosinetriphosphatase. *Biochemistry* 25:696-703

10. Branden CI. 1980. Relation between structure and function of alpha/beta-proteins. *Quart. Rev. Biophys.* 13:317-38

11. Castellani L, Hardwicke PM. 1983. Crystalline structure of sarcoplasmic reticulum from scallop. *J. Cell. Biol.* 97:557-61

12. Champeil P, Henao F, de Foresta B. 1997. Dissociation of Ca^{2+} from sarcoplasmic reticulum Ca^{2+}-ATPase and changes in fluorescence of optically selected Trp residues. Effects of KCl and NaCl and implications for substeps in Ca^{2+} dissociation. *Biochemistry* 36:12383-93

13. Champeil P, Henao F, Lacapere JJ, McIntosh DB. 2001. A remarkably stable phosphorylated form of Ca^{2+}-ATPase prepared from Ca^{2+}-loaded and fluorescein isothiocyanate-labeled sarcoplasmic reticulum Vesicles. *J. Biol. Chem.* 276:5795-803

14. Cheong G-W, Young HS, Ogawa H, Toyoshima C, Stokes DL. 1996. Lamellar stacking in three-dimensional crystals of Ca^{2+}-ATPase from sarcoplasmic reticulum. *Biophys. J.* 70:1689-99

15. Clarke DM, Loo TW, Inesi G, MacLennan DH. 1989. Location of high affinity Ca^{2+}-binding sites within the predicted transmembrane domain of the sarcoplasmic reticulum Ca^{2+}-ATPase. *Nature* 339:476-78

16. Collet J-F, van Schaftingen E, Stroobant V. 1998. A new family of phosphotransferases related to P-type ATPases. *Trends Biol. Sci.* 23:284

17. Cyrklaff M, Auer M, Kühlbrandt W, Scarborough GA. 1995. 2-D structure of the *Neurospora crassa* plasma membrane ATPase as determined by electron cryomicroscopy. *EMBO J.* 14:1854-57

18. Daiho T, Kanazawa T. 1994. Reduction of disulfide bonds in sarcoplasmic reticulum Ca^{2+}-ATPase by dithiothreitol causes inhibition of phosphoenzyme isomerization in catalytic cycle. This reduction requires binding of both purine nucleotide and Ca^{2+} to enzyme. *J. Biol. Chem.* 269:11060-64
19. Danko S, Daiho T, Yamasaki K, Kamidochi M, Suzuki H, et al. 2001. ADP-insensitive phosphoenzyme intermediate of sarcoplasmic reticulum Ca^{2+}-ATPase has a compact conformation resisitant to proteinase K, V8 protease and trypsin. *FEBS Lett.* 489:277-82
20. Danko S, Yamasaki K, Daiho T, Suzuki H, Toyoshima C. 2001. Organization of cytoplasmic domains of sarcoplasmic reticulum Ca^{2+}-ATPase in E_1P and E_1ATP states: a limited proteolysis study. *FEBS Lett.* 505:129-35
21. deMeis L, Vianna A. 1979. Energy Interconversion by the Ca^{+}-dependent ATPase of the Sarcoplasmic Reticulum. *Annu. Rev. Biochem.* 48:275-92
22. Dupont Y, Bennett N. 1982. Vanadate inhibition of the Ca^{2+}-dependent conformational change of the sarcoplasmic reticulum Ca^{2+}-ATPase. *FEBS Lett.* 139:237-40
23. Dux L, Martonosi A. 1983. Ca^{2+}-ATPase membrane crystals in sarcoplasmic reticulum. The effect of trypsin digestion. *J. Biol. Chem.* 258:10111-15
24. Dux L, Martonosi A. 1983. Two-dimensional arrays of proteins in sarcoplasmic reticulum and purified Ca^{2+}-ATPase vesicles treated with vanadate. *J. Biol. Chem.* 258:2599-603
25. Dux L, Pikula S, Mullner N, Martonosi A. 1987. Crystallization of Ca^{2+}-ATPase in detergent-solubilized sarcoplasmic reticulum. *J. Biol. Chem.* 262:6439-42
26. Ebashi S, Lipmann F. 1962. Adenosine triphosphate-linked concentration of calcium ions in a particulate fraction of rabbit muscle. *J. Cell. Biol.* 14:389-400
27. Einholm AP, Vilsen B, Andersen JP. 2002. *Functional consequences of charge-reversals of acidic residues in M1 of the SR Ca-ATPase*. Presented at the 10th International conference on Na,K-ATPase and related cation pumps, Elsinore, Denmark
28. Fagan MJ, Saier MH. 1994. P-type ATPases of eukaryotes and bacteria: sequence analysis and construction of phylogenetic trees. *J. Mol. Evol.* 38:57-99
29. Fukushima Y, Post RL. 1978. Binding of divalent cation to phosphoenzyme of sodium- and potassium-transport adenosine triphosphatase. *J. Biol. Chem.* 253:6853-62
30. Gadsby DC, Rakowski RF, De Weer P. 1993. Extracellular access to the Na, K pump: Pathway similar to ion channel. *Science* 260:100-103
31. Girardet JL, Dupont Y. 1992. Ellipticity changes of the sarcoplasmic reticulum Ca^{2+}-ATPase induced by cation binding and phosphorylation. *FEBS Lett.* 296:103-106
32. Glynn I. 1985. The Na^{+},K^{+}-transporting adenosine triphophatase. In *The Enzymes of Biological Membranes*, ed. A Martonosi, pp. 35-114. New York: Plenum
33. Goldshleger R, Karlish SJ. 1999. The energy transduction mechanism of Na,K-ATPase studied with iron-catalyzed oxidative cleavage. *J. Biol. Chem.* 274:16213-21
34. Greeves M, Holmes KC. 1999. Structural mechanism of muscle contraction. *Ann. Rev. Biochemistry* 687:687-728
35. Hardwicke PMD, Bozzola JJ. 1989. Effect of phosphorylation on scallop sarcoplasmic reticulum. *J. Musc. Res. Cell. Motil.* 10:245-253
36. Hasselbach W, Oetliker H. 1983. Energetics and electrogenecity of the sarcoplasmic reticulum calcium pump. *Annu. Rev. Physiol.* 45:325-29

37. Hebert H, Purhonen P, Vorum H, Thomsen K, Maunsbach AB. 2001. Three-dimensional structure of renal Na,K-ATPase from cryo-electron microscopy of two-dimensional crystals. *J. Mol. Biol.* 314:479-94
38. Henao F, Delavoie F, Lacapere JJ, McIntosh DB, Champeil P. 2001. Phosphorylated Ca^{2+}-ATPase stable enough for structural studies. *J. Biol. Chem.* 276:24284-85
39. Hisano T, Hata Y, Fujii T, Liu J-Q, Kurihara T, et al. 1996. Crystal structure of L-2-haloacid dehalogenase from *Pseudomonas* sp. YL. *J. Biol. Chem.* 271:20322-30
40. Houdusse A, Sweeney HL. 2001. Myosin motors: missing structures and hidden springs. *Curr. Opin. Struct. Biol.* 11:182-94
41. Huang S, Squier TC. 1998. Enhanced rotational dynamics of the phosphorylation domain of the Ca-ATPase upon calcium activation. *Biochemistry* 37:18064-73
42. Imamura Y, Kawakita M. 1989. Purification of limited tryptic fragments of Ca^{2+},Mg^{2+}-adenosine triphosphatase of the sarcoplasmic reticulum and identification of conformation-sensitive cleavage sites. *J. Biochem.* 105:775-81
43. Imamura Y, Saito K, Kawakita M. 1984. Conformational change of Ca^{2+},Mg^{2+}-adenosine triphosphatase of sarcoplasmic reticulum upon binding of Ca2+ and adenyl-5'-yl-imidodiphosphate as detected by trypsin sensitivity analysis. *J. Biochem.* 95:1305-13
44. Inesi G. 1985. Mechanism of Calcium Transport. *Annu. Rev. Physiol.* 47:573-601
45. Inesi G, Lewis D, Nikic D, Hussain A, Kirtley ME. 1992. Long-range intramolecular linked functions in the calcium transport ATPase. *Adv. Enzym.* 65:185-215
46. Jencks WP. 1989. How Does a Calcium Pump Pump Calcium. *J. Biol. Chem.* 264: 18855-58
47. Jencks WP. 1989. Utilization of binding energy and coupling rules for active transport and other coupled vectorial processes. *Methods Enzymol.* 171:145-64
48. Jorge-Garcia I, Bigelow DJ, Inesi G, Wade JB. 1988. Effect of urea on the partial reactions and crystallization pattern of sarcoplasmic reticulum adenosine triphosphatase. *Arch. Biochem. Biophys.* 265:82-90
49. Jorgensen PL, Andersen JP. 1988. Structural basis for E_1-E_2 conformational transitions in Na,K-pump and Ca-pump proteins. *J. Membr. Biol.* 103:95-120
50. Jorgensen PL, Jorgensen JR, Pedersen PA. 2001. Role of conserved TGDGVND-loop in Mg^{2+} binding, phosphorylation, and energy transfer in Na,K-ATPase. *J. Bioenerg. Biomembr.* 33:367-77
51. Kuehlbrandt W, Zeelen J, Dietrich J. 2002. Structure, mechanism, and regulation of the neurospora plasma membrane H^+-ATPase. *Science* 297:1692-96
52. Lauger P. 1991. *Electrogenic Ion Pumps*, pp. 240-46. Sunderland, MA: Sinauer.
53. Lee SY, Cho HS, Pelton JG, Yan D, Berry EA, et al. 2001. Crystal structure of activated CheY. Comparison with other activated receiver domains. *J. Biol. Chem.* 276:16425-31
54. Lutsenko S, Kaplan JH. 1995. Organization of P-type ATPases: significance of structural diversity. *Biochemistry* 34:15607-13
55. MacLennan DH, Brandl CJ, Korczak B, Green NM. 1985. Amino-acid sequence of a Ca^{2+} + Mg^{2+}- dependent ATPase from rabbit muscle sarcoplasmic reticulum, deduced from its complementary DNA sequence. *Nature* 316:696-700
56. Makinose M. 1973. Possible functional states of the enzyme of the sarcoplasmic calcium pump. *FEBS Lett.* 37:140-43

57. Martonosi A, Taylor KA, Varga S, Ping Ting-Beall H. 1987. The molecular structure of sarcoplasmic reticulum. In *Electron microscopy of proteins: Membranous structures*, ed. JR Harris, RW Horne, pp. 255-376. London: Academic Press
58. Matlack KE, Misselwitz B, Plath K, Rapoport TA. 1999. BiP acts as a molecular ratchet during posttranslational transport of prepro-alpha factor across the ER membrane. *Cell* 97:553-64
59. Maunsbach AB, Skriver E, Hebert H. 1991. Two-dimensional crystals and three-dimensional structure of Na,K-ATPase analyzed by electron microscopy. *Soc. Gen. Physiol. Ser.* 46:159-72
60. Maurer A, Fleischer S. 1984. Decavanadate is responsible for vanadate-induced two-dimensional crystals in sarcoplasmic reticulum. *J. Bioenerg. Biomembr.* 16:491-505
61. McIntosh D. 1998. The ATP binding sites of P-type ion transport ATPases. *Adv. Mol. Cell Biol.* 23A:33-99
62. Mintz E, Guillain F. 1997. Ca^{2+} transport by the sarcoplasmic reticulum ATPase. *Biochim. Biophys. Acta* 1318:52-70
63. Mohraz M, Yee M, Smith PR. 1985. Novel crystalline sheets of Na,K-ATPase induced by phospholipase A2. *J. Ultrastruct. Res.* 93:17-26
64. Moller JV, Juul B, le Maire M. 1996. Structural organization, ion transport, and energy transduction of ATPases. *Biochim. Biophys. Acta* 1286:1-51
65. Moller JV, Lenoir G, Marchand C, Montigny C, Le Maire M, et al. 2002. Calcium transport by sarcoplasmic reticulum Ca^{2+}-ATPase : role of the A-domain and its C-terminal link with the transmembrane region. *J. Biol. Chem.* 22: in press
66. Murphy AJ. 1978. Effects of divalent cations and nucleotides on the reactivity of the sulfhydryl groups of sarcoplasmic reticulum membranes. Evidence for structural changes occurring during the calcium transport cycle. *J. Biol. Chem.* 253:385-89
67. Murphy AJ, Coll RJ. 1992. Fluoride binding to the calcium ATPase of sarcoplasmic reticulum converts its transport sites to a low affinity, lumen-facing form. *J. Biol. Chem.* 267:16990-94
68. Ogawa H, Stokes DL, Sasabe H, Toyoshima C. 1998. Structure of the Ca^{2+} pump of sarcoplasmic reticulum: a view along the lipid bilayer at 9-Å resolution. *Biophys. J.* 75:41-52
69. Okamoto K, Brinker A, Paschen SA, Moarefi I, Hayer-Hartl M, et al. 2002. The protein import motor of mitochondria: a targeted molecular ratchet driving unfolding and translocation. *EMBO J.* 21:3659-71
70. Oster G, Wang H. 1999. ATP synthase: two motors, two fuels. *Structure* 7:R67-R72
71. Patchornik G, Goldshleger R, Karlish SJ. 2000. The complex ATP-Fe^{2+} serves as a specific affinity cleavage reagent in ATP-Mg^{2+} sites of Na,K-ATPase: altered ligation of Fe^{2+} (Mg^{2+}) ions accompanies the E_1P -> E_2P conformational change. *Proc. Natl. Acad. Sci.* 97:11954-59
72. Pedersen PA, Jorgensen JR, Jorgensen PL. 2000. Importance of conserved alpha -subunit segment 709GDGVND for Mg^{2+} binding, phosphorylation, and energy transduction in Na,K-ATPase. *J. Biol. Chem.* 275:37588-95
73. Pick U. 1982. The interaction of vanadate ions with the Ca-ATPase from sarcoplasmic reticulum. *J. Biol. Chem.* 257:6111-19
74. Pick U, Karlish SJD. 1980. Indications for an oligomeric structure and for conformational changes in sarcoplasmic reticulum Ca^{2+}-ATPase labelled selectively with fluorescein. *Biochim. Biophys. Acta* 626:255-61

75. Post R, Merritt C, Kinsolving C, Albright C. 1960. Membrane adenosine triphosphatase as a participant in the active transport of sodium and potassium in the human erythrocyte. *J. Biol. Chem.* 235:1796-1802
76. Post RL, Kume S. 1973. Evidence for an aspartyl phosphate residue at the active site of sodium and potassium ion transport adenosine triphosphatase. *J. Biol. Chem.* 248:6993-7000
77. Rabon E, Wilke M, Sachs G, Zampighi G. 1986. Crystallization of the gastric H,K-ATPase. *J. Biol. Chem.* 261:1434-39
78. Reinstein J, Jencks WP. 1993. The binding of ATP and Mg^{2+} to the calcium adenosinetriphosphatase of sarcoplasmic reticulum follows a random mechanism. *Biochemistry* 32:6632-42
79. Rice WJ, Young HS, Martin DW, Sachs JR, Stokes DL. 2001. Structure of Na^+,K^+-ATPase at 11 Å resolution: comparison with Ca^{2+}-ATPase in E_1 and E_2 states. *Biophys. J.* 80:2187-97
80. Ross DC, Davidson GA, McIntosh DB. 1991. Mechanism of inhibition of sarcoplasmic reticulum Ca^{2+}-ATPase by active site cross-linking. *J. Biol. Chem.* 266:4613-21
81. Sagara Y, Wade JB, Inesi G. 1992. A conformational mechanism for formation of a dead-end complex by the sarcoplasmic reticulum ATPase with thapsigargin. *J. Biol. Chem.* 267:1286-92
82. Seekoe T, Peall S, McIntosh DB. 2001. Thapsigargin and dimethyl sulfoxide activate medium P_i <-> HOH oxygen exchange catalyzed by sarcoplasmic reticulum Ca^{2+}-ATPase. *J. Biol. Chem.* 276:46737-44
83. Shi D, Hsiung H-H, Pace RC, Stokes DL. 1995. Preparation and analysis of large, flat crystals of Ca^{2+}-ATPase for electron crystallography. *Biophys. J.* 68:1152-62
84. Shi D, Lewis MR, Young HS, Stokes DL. 1998. Three-dimensional crystals of Ca^{2+}-ATPase from sarcoplasmic reticulum: merging electron diffraction tilt series and imaging the (h, k, 0) projection. *J. Mol. Biol.* 284:1547-64
85. Skou JC. 1957. The influence of some cations on an adenosine triphosphatase from peripheral nerves. *Biochim. Biophys. Acta* 23:394-401
86. Skriver E, Kaveus U, Hebert H, Maunsbach AB. 1992. Three-dimensional structure of Na,K-ATPase determined from membrane crystals induced by cobalt-tetrammine-ATP. *J. Struc. Biol.* 108:176-85
87. Skriver E, Maunsbach AB, Jorgensen PL. 1981. Formation of two-dimensional crystals in pure membrane-bound Na^+/K^+-ATPase. *FEBS Lett.* 131:219-22
88. Stokes DL, Auer M, Zhang P, Kuehlbrandt W. 1999. Comparison of H^+-ATPase and Ca^{2+}-ATPase suggests that a large conformational change initiates P-type ion pump reaction cycles. *Curr. Biol.* 9:672-79
89. Stokes DL, Green NM. 1990. Three-dimensional crystals of Ca-ATPase from sarcoplasmic reticulum: symmetry and molecular packing. *Biophys. J.* 57:1-14
90. Stokes DL, Green NM. 2000. Modeling a dehalogenase fold into the 8-Å density map for Ca^{2+}-ATPase defines a new domain structure. *Biophys. J.* 78:1765-76
91. Stokes DL, Lacapere J-J. 1994. Conformation of Ca^{2+}-ATPase in two crystal forms: Effects of Ca^{2+}, thapsigargin, AMP-PCP, and Cr-ATP on crystallization. *J. Biol. Chem.* 269:11606-13
92. Strock C, Cavagna M, Peiffer WE, Sumbilla C, Lewis D, Inesi G. 1998. Direct demonstration of Ca^{2+} binding defects in sarco-endoplasmic reticulum Ca^{2+} ATPase mutants overexpressed in COS-1 cells transfected with adenovirus vectors. *J. Biol. Chem.* 273:15104-9

93. Toyoshima C, Nakasako M, Nomura H, Ogawa H. 2000. Crystal structure of the calcium pump of sarcoplasmic reticulum at 2.6 Å resolution. *Nature* 405:647-55
94. Toyoshima C, Nomura H. 2002. Structural changes in the calcium pump accompanying the dissociation of calcium. *Nature* 418:605-11
95. Toyoshima C, Sasabe H, Stokes DL. 1993. Three-dimensional cryo-electron microscopy of the calcium ion pump in the sarcoplasmic reticulum membrane. *Nature* 362:469-71
96. Varga S, Csermely P, Martonosi A. 1985. The binding of vanadium (V) oligoanions to sarcoplasmic reticulum. *Eur. J. Biochem.* 148:119-26
97. Wakabayashi S, Imagawa T, Shigekawa M. 1990. Does fluorescence of 4-nitrobenzo-2-oxa-1,3-diazole incorporated into sarcoplasmic reticulum ATPase monitor putative E_1-E_2 conformational transition? *J. Biochem.* 107:563-71
98. Wakabayashi S, Shigekawa M. 1984. Role of divalent cation bound to phosphoenzyme intermediate of sarcoplasmic reticulum ATPase. *J. Biol. Chem.* 259:4427-36
99. Wang W, Cho HS, Kim R, Jancarik J, Yokota H, et al. 2002. Structural characterization of the reaction pathway in phosphoserine phosphatase: crystallographic "snapshots" of intermediate states. *J. Mol. Biol.* 319:421-31
100. Wang W, Kim R, Jancarik J, Yokota H, Kim SH. 2001. Crystal structure of phosphoserine phosphatase from Methanococcus jannaschii, a hyperthermophile, at 1.8 A resolution. *Structure* 9:65-71
101. Watanabe T, Inesi G. 1982. The use of 2',3'-O-(2,4,6-trinitrophenyl) adenosine 5'-triphosphate for studies of nucleotide interaction with sarcoplasmic reticulum vesicles. *J. Biol. Chem.* 257:11510-16
102. Wictome M, Khan YM, East JM, Lee AG. 1995. Binding of sesquiterpene lactone inhibitors to the Ca^{2+}-ATPase. *Biochem. J.* 310:859-68
103. Xian Y, Hebert H. 1997. Three-dimensional structure of the porcine gastric H,K-ATPase from negatively stained crystals. *J. Struct. Biol.* 118:169-77
104. Xu C, Rice WJ, He W, Stokes DL. 2002. A structural model for the catalytic cycle of Ca^{2+}-ATPase. *J. Mol. Biol.* 316:201-11
105. Young H, Xu C, Zhang P, Stokes D. 2001. Locating the thapsigargin binding site on Ca^{2+}-ATPase by cryoelectron microscopy. *J. Mol. Biol.* 308:231-40
106. Zhang P, Toyoshima C, Yonekura K, Green NM, Stokes DL. 1998. Structure of the calcium pump from sarcoplasmic reticulum at 8 Å resolution. *Nature* 392:835-39
107. Zhang Z, Sumbilla C, Lewis D, Inesi G. 1993. High sensitivity to site directed mutagenesis of the peptide segment connecting phosphorylation and Ca binding domainsin the Ca transport ATPase. *FEBS Lett.* 335:261-64
108. Zhao R, Collins EJ, Bourret RB, Silversmith RE. 2002. Structure and catalytic mechanism of the E. coli chemotaxis phosphatase CheZ. *Nat. Struct. Biol.* 9:570-575

Table I. Reaction Intermediates of Ca^{2+}-ATPase and their Chemical Modifications

Reaction Intermediate	Physiological Ligands[a]	Stabilizing Ligand	chemical modifications[b]
E_2H[c]		pH6/Tg	2D crystals scallop/NaK(11, 79) **P-A**: Fe cleavage TGES (71) **P-N**: SH/DTNB ++ (66) glut. crosslink (80) **A**: T2 cleavage 100 V8/PK cleavage 100 (19, 20) **M**: TG binding (81)
↓	- nH^+		
E_1		pH7-8	
↓	+ $2Ca^{++}$		
E_1Ca_2[c]		Ca	3D crystals (91) **P-N**: SH/DTNB +++ (66) glut. crosslink slow (80) **A**: T2 cleavage 210 V8/PK cleavage 110 (20)
↓	+ ATP		
$E_1MgATPCa_2$		AMPPNP/ AMPPCP	**P**: Mg^{2+} fast exchange (78) **P-N**: SH/DTNB ++ (66) no glut. crosslink (80) **A**: T2 cleavage 60 V8/PK cleavage 10 (20)
↓			
$E_1MgP(Ca_2)ADP$		AlF_4^-ADP $CrATP/Ca^{2+}$	**P-N**: SH/DTNB + (66) glut. crosslink fast (80) **A**: T2 cleavage 70 V8/PK cleavage 0 (20) **M**: TG+CrATP slow Ca^{2+} off (81)
↓	- ADP		
E_2MgPCa_2			
↓	- $2Ca^{++}$ + H^+		
E_2MgPH[d]		BeF_3/VO_3 CrATP	2D crystals $V_{10}O_{29}/VO_4$ (91) **P-N**: no glut. crosslink (80) **P-A**: Fe cleaves TGES (71) **A**: T2 cleavage 0 V8/PK cleavage 0 (19)
↓	+ H_2O		
E_2MgP_iH[e]		Mg_2F_4	**P-N**: SH/DTNB + (67)
↓	- Mg,-P_i		
E_2H			

More chemical modifications[f]

unphosphorylated species (E2 ... E1·Ca_2): **P**: Mg^{2+} fast exchange (78); **N**: TNPAMP low fluor. (9)

phosphorylated species ($E1MgP(Ca_2).ADP$ ... E2MgP): **P**: Mg^{2+} occluded (98); **N**: TNPAMP high fluor. (9)

E1 species: (E1 ... $E1MgP(Ca_2).ADP$): **P**: NDB-Cys344 high fluor. (97), **P-A**: no Fe cleavage TGES (33, 71), **N**: FITC low fluor. (74)

E2 species: (E2MgP.2Ca ... E2): **P**: NBD-cys344 low fluor. (97), **N**: FITC high fluor. (74)

[a] Ligands gained or lost at each step of the reaction cycle.
[b] Results for each intermediate, with relevant domains indicated by bold type. The numbers listed for proteolytic cleavages are rate constants relative to unliganded species in EGTA and the pluses listed for DTNB indicate the relative accessibility of cysteines.
[c] existing X-ray structure
[d] existing EM structure
[e] X-ray structure in progress
[f] Results not specific for individual intermediates, but for neighboring intermediates in the reaction cycle.
abbreviations: TG: thapsigargin, T2: tryptic cleavage site at R^{198}, V8/PK: V8 protease and proteinase K cleavage sites, glut: glutaraldehyde, fluor: fluorescence, FITC: fluorescein isothiocyanate, NBD: 4-nitro-2,1,3-benzoxadiazole, DTNB: 5,5'-dithiobis-2-nitrobenzoate

FIGURE LEGENDS

Figure 1. Topology of Ca^{2+}-ATPase indicating the location of key functional sites described in the text. Sequence motifs are indicated by the single-letter code with numbers corresponding to the sequence of rabbit fast-twitch muscle Ca^{2+}-ATPase (SERCA1). Cytoplasmic domains are denoted N, P and A; P1, P4a,b, and P6 correspond to particular helices within the P domain. Shaded helices in the P and N domains are in front of the central sheet, whereas unshaded helices are behind. Proteolytic sites are indicated as T1 and T2 for trypsin and PK for proteinase K. Minor loops between transmembrane helices are indicated as L67, L78 and PLB indicates the binding site for phospholamban.

Figure 2. Ribbon diagrams of Ca^{2+}-ATPase and H^+-ATPase in different conformations. Structures for $E_1 \cdot Ca_2$ (A; PDB code 1EUL) and $E_2 \cdot TG$ (C; PDB code 1IWO) were determined by x-ray crystallography and those for H^+-ATPase (B; PDB code 1MHS) and $E_2 \cdot VO_4$ (D; PDB code 1KJU) were fitted to cryoEM maps. Several functional sites are indicated (cf., Fig. 1) and cytoplasmic domains are color coded green (N), magenta (P) and yellow (A). Transmembrane domain (TM) is grey except for M4 and M5 which are blue. Figure made with SPDBV and rendered with POV-Ray.

Figure 3. Stereo view of calcium binding residues from Ca^{2+}-ATPase in $E_1 \cdot Ca_2$ (A) and $E_2 \cdot TG$ states (B). Calcium ions are colored magenta. Dramatic changes in the backbone of M6 and the side chains of E^{309} and E^{58} occur during calcium binding. Figure made with PyMOL.

Figure 4. Stereo view of phosphorylation site of Ca^{2+}-ATPase (A) and phosphoserine phosphatase (B; PDB code 1J97), the latter with $Mg \cdot BeF_3^-$ forming an analogue of the aspartyl phosphate. $E_1 \cdot Ca_2$ and $E_2 \cdot TG$ structures are overlaid in A with ribbons respectively colored magenta and blue; side chains for $E_2 \cdot TG$ are colored cyan and, except for small changes in the $DGVND^{707}$ loop, are in virtually identical positions in the two Ca^{2+}-ATPase structures. Compared to phosphoserine phosphatase, this same loop is considerably farther from $Mg \cdot BeF_3^-$ (magnesium colored magenta and fluoride in orange), suggesting substantial movements upon phosphorylation of Ca^{2+}-ATPase. The side chain of D^{351} would also be expected to swivel up to match the position of D^{11} in phosphoserine phosphatase. Figure made with SPDBV and POV-Ray.

Figure 5. Comparison of $E_2 \cdot TG$ and $E_2 \cdot VO_4$ structures with particular reference to the interface between A and P domains. Molecular envelopes were determined by cryoEM of the $E_2 \cdot VO_4$ state and, after fitting, represent the basis for the E_2VO_4 structure (A); due to movements of N and A domains $E_2 \cdot TG$ coordinates produce a poor fit (B). These movements are primarily a result of differences in the A-P domain interface, shown in stereo for $E_2 \cdot VO_4$ (C) and $E_2 \cdot TG$ (D). Although the domains are colored according to Fig. 2, the $TGES^{184}$ and $DGVND^{707}$ loops are colored red and blue, respectively, to highlight their different interactions in these two states. Figure made with SPDBV and POV-Ray.

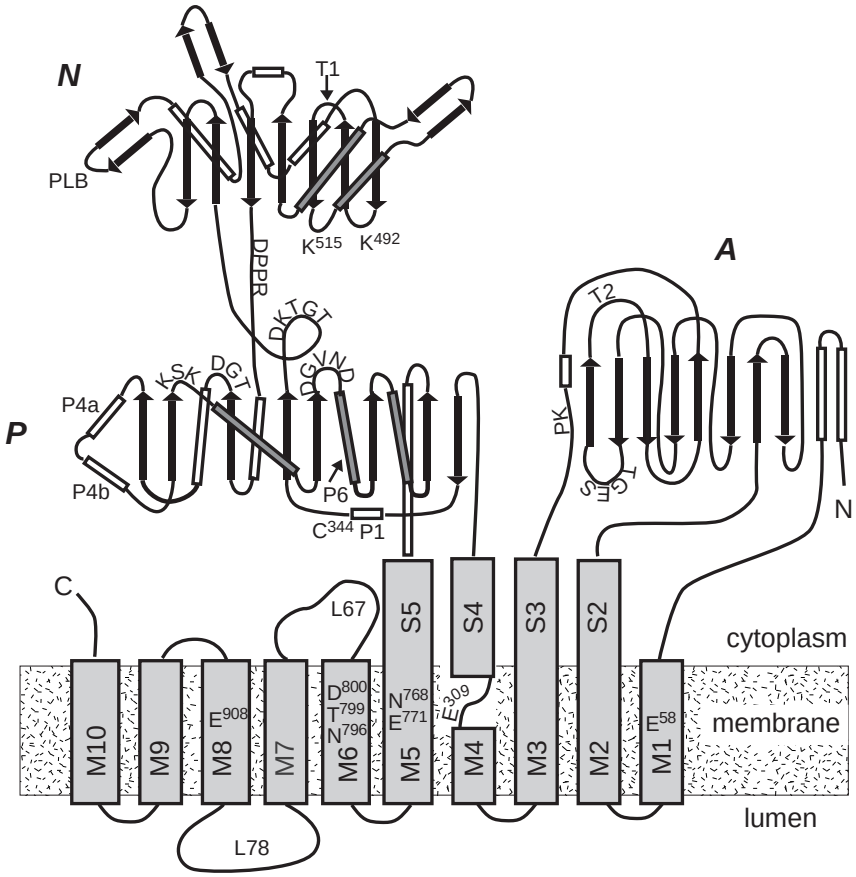
N
T1
PLB
K515
K492
DPPR
DKTGT
A
T2
PK
TGES
N
P
P4a
KSK
DGT
DGVND
P4b
P6
C344
P1
C
L67
S5
S4
S3
S2
cytoplasm
M10
M9
M8
M7
M6
M5
M4
M3
M2
M1
D800
T799
N796
N768
E771
E309
E908
E58
membrane
lumen
L78

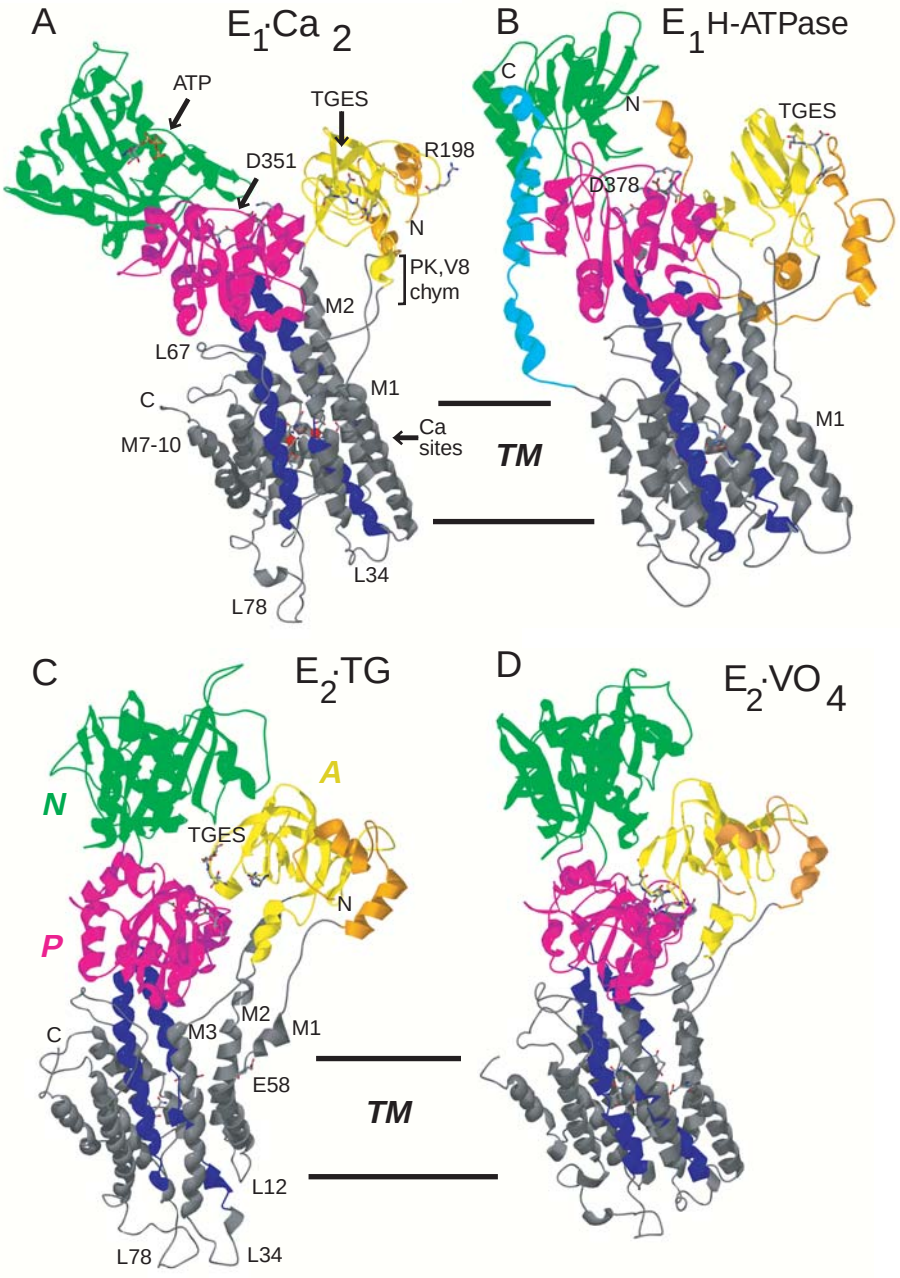
A
E1·Ca 2
ATP
TGES
D351
R198
N
PK,V8
chym
M2
L67
M1
C
M7-10
Ca
sites
TM
L34
L78
B
E1H-ATPase
C
N
TGES
D378
M1
C
E2:TG
N
A
TGES
N
P
M2
M1
M3
C
E58
TM
L12
L78
L34
D
E2·VO 4

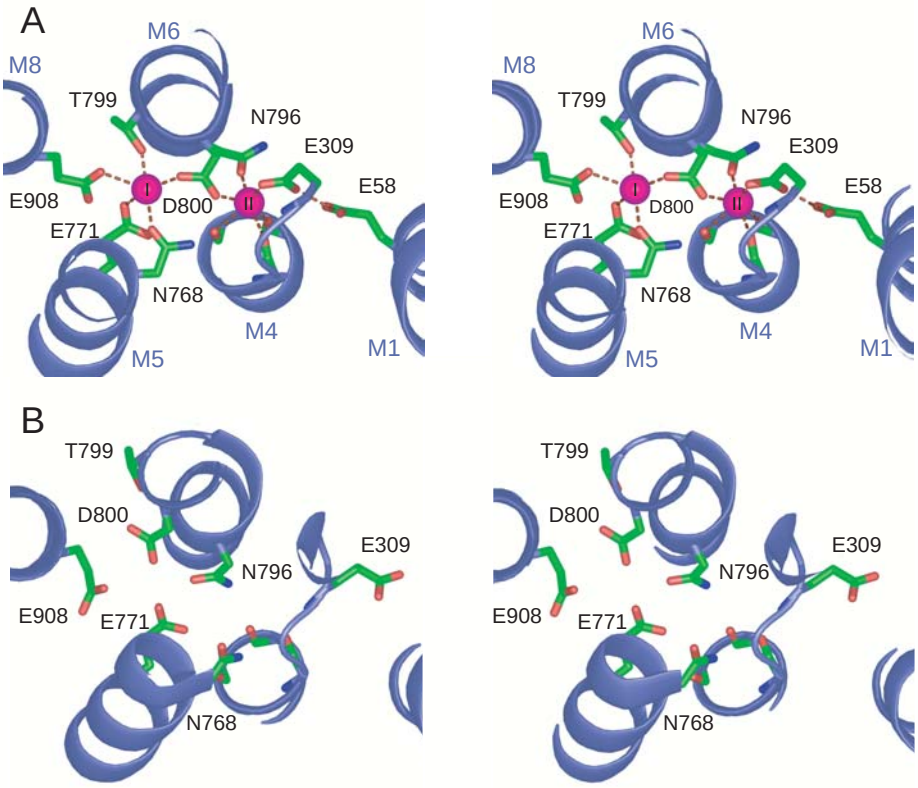
A
M6
M8
T799
N796
E309
E58
E908
I
D800
II
E771
N768
M4
M5
M1
B
T799
D800
E309
N796
E908
E771
N768

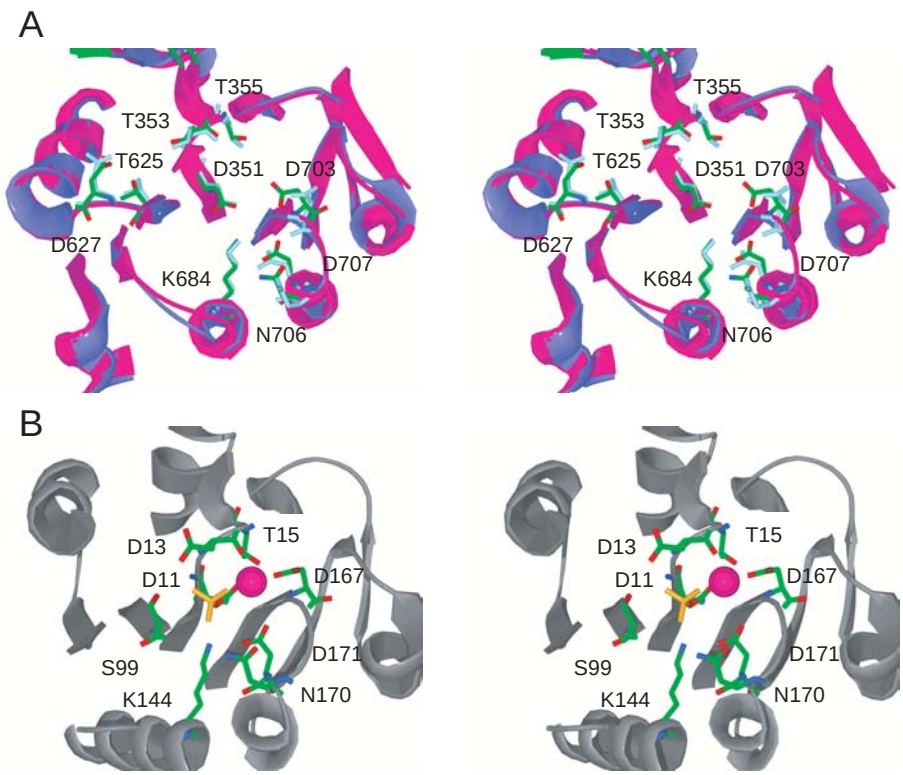
A
T355
T353
T625
D351
D703
D627
K684
D707
N706
T355
T353
T625
D351
D703
D627
K684
D707
N706
B
D13
T15
D11
D167
S99
D171
K144
N170
D13
T15
D11
D167
S99
D171
K144
N170

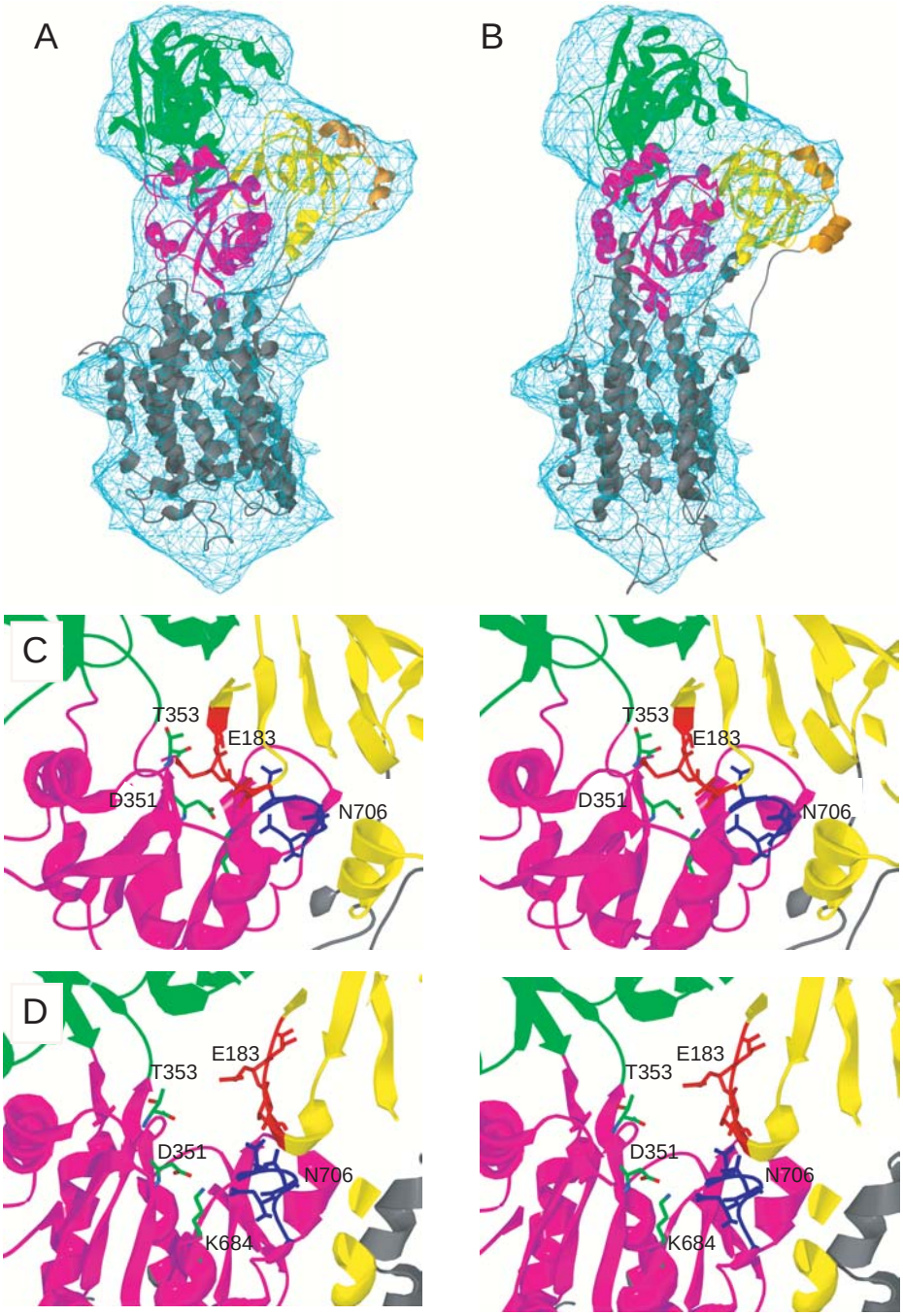
A
B
C
T353
E183
D351
N706
T353
E183
D351
N706
D
E183
T353
D351
N706
K684
E183
T353
D351
N706
K684